Supplementary Information

Surmounting interband threshold limit by the hot electron excitation of multi-metallic plasmonic AgAuCu NPs for the UV photodetector application

Shusen Lin,[a] Rakesh Kulkarni,[a] Rutuja Mandavkar, [a] Md Ahasan Habib, [a] Shalmali Burse, [a] Sundar Kunwar*[a,b] and Jihoon Lee**[a]

[a] Department of Electronic Engineering, College of Electronics and Information, Kwangwoon University, Nowon-gu Seoul, 01897, South Korea.

[b] Center for Integrated Nanotechnologies (CINT), Los Alamos National Laboratory, Los Alamos, New Mexico 87545, USA

Correspondence e-mail: sundar@lanl.gov (S. Kunwar)*, jihoonlee@kw.ac.kr (J. Lee)**

Simulation details

To simulate the electromagnetic field distribution of AgCu, AuCu, AgAuCu alloy NPs and MoS_2/AgAuCu hybrid configuration, the finite difference time domain (FDTD) solution (Lumerical Solutions, Canada) was adapted. In this work, the total-field scattered-field (TFSF) source was used to analyze the scattering of nanoparticles and hybrid configuration. The TFSF source separates the computation region into the total field and scattered field regions. The scattering and absorption monitors were used to determine the excitation power, which is based on excitation = absorption + scattering. The DFT monitors were placed with the same dimension to study the near e-field profile and to avoid the difference in the spectrum. The perfectly matched layer (PML) boundary and the nanostructure were designed to allow the radiation propagations out of the computational regions without disturbing the fields inside. The PML boundary absorbs the electromagnetic wave and demonstrated more effectiveness for the radiation absorption. The mesh size with 0.2 nm in X, Y, and Z were used to improve the accuracy. The refractive index of Ag, Au and Cu were fitted by the Johnson's model [1]. The refractive index of MoS_2 nanoflakes was fitted by the Beal and Hughes model [2]separately. The simulated nanostructure exhibited an electromagnetic field with the defined frequencies, which shows a good agreement with alloy NP photoresponse.

Bare GaN characterizations

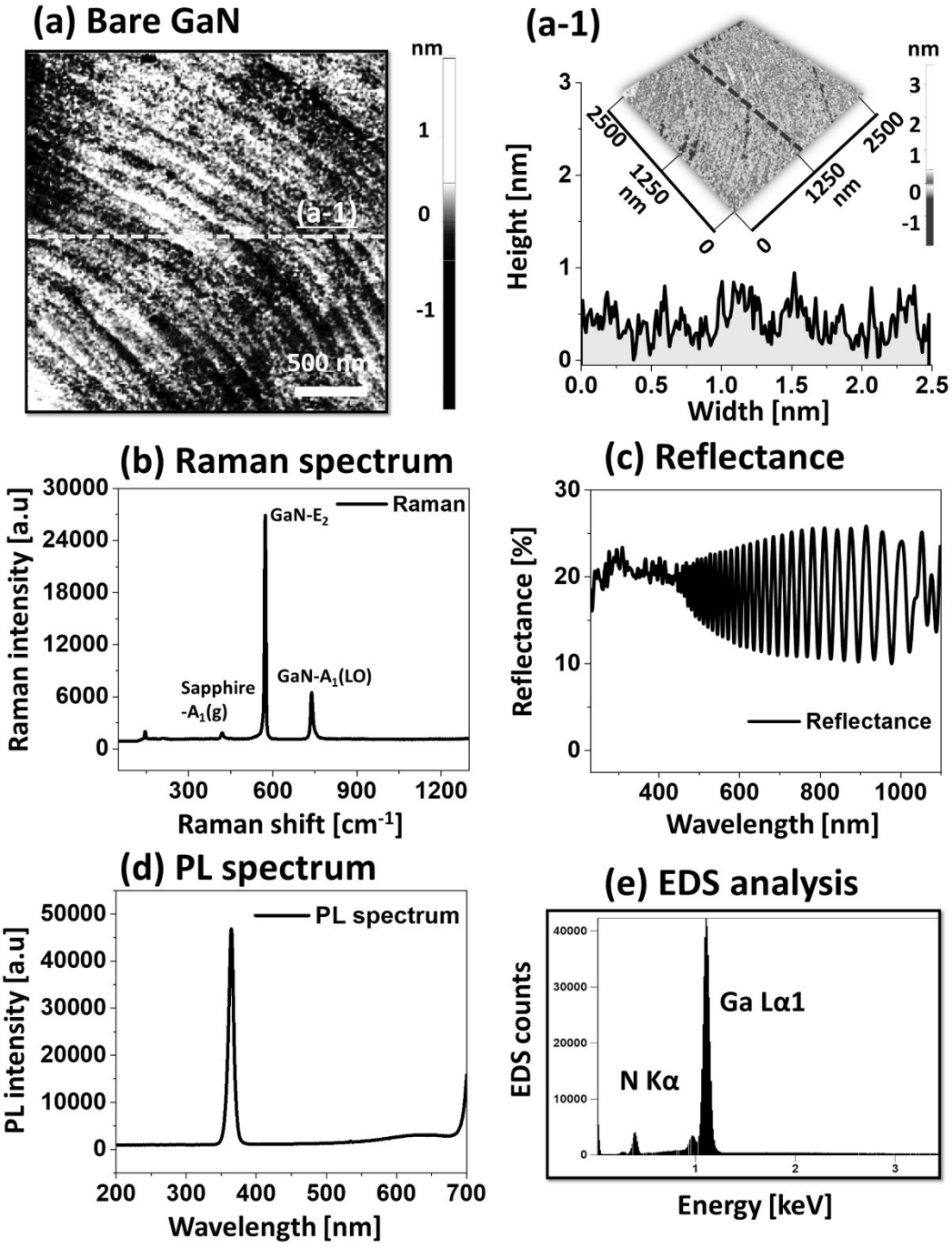

Figure S1: (a) AFM top-view of bare GaN substrate after degassing at 300 °C for 30 min, showing the atomic steps after the oxide removal. (a-1) Corresponding AFM side-view and cross-sectional line-profile. (b) – (e) Raman, reflectance, photoluminescence (PL) and EDS spectra of bare GaN respectively.

Multi-layer schematics

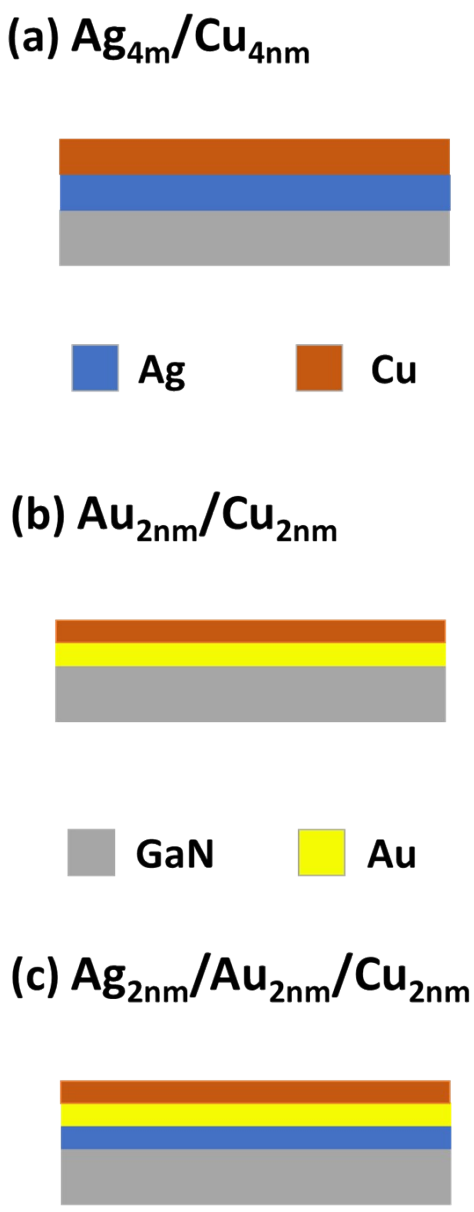

Figure S2: (a) – (c) Schematic of Ag/Cu, Au/Cu, and Ag/Au/Cu metal films by sputtering. Subscripts indicate the multilayer thickness.

Characterization of $Ag_1Au_1Cu_1$

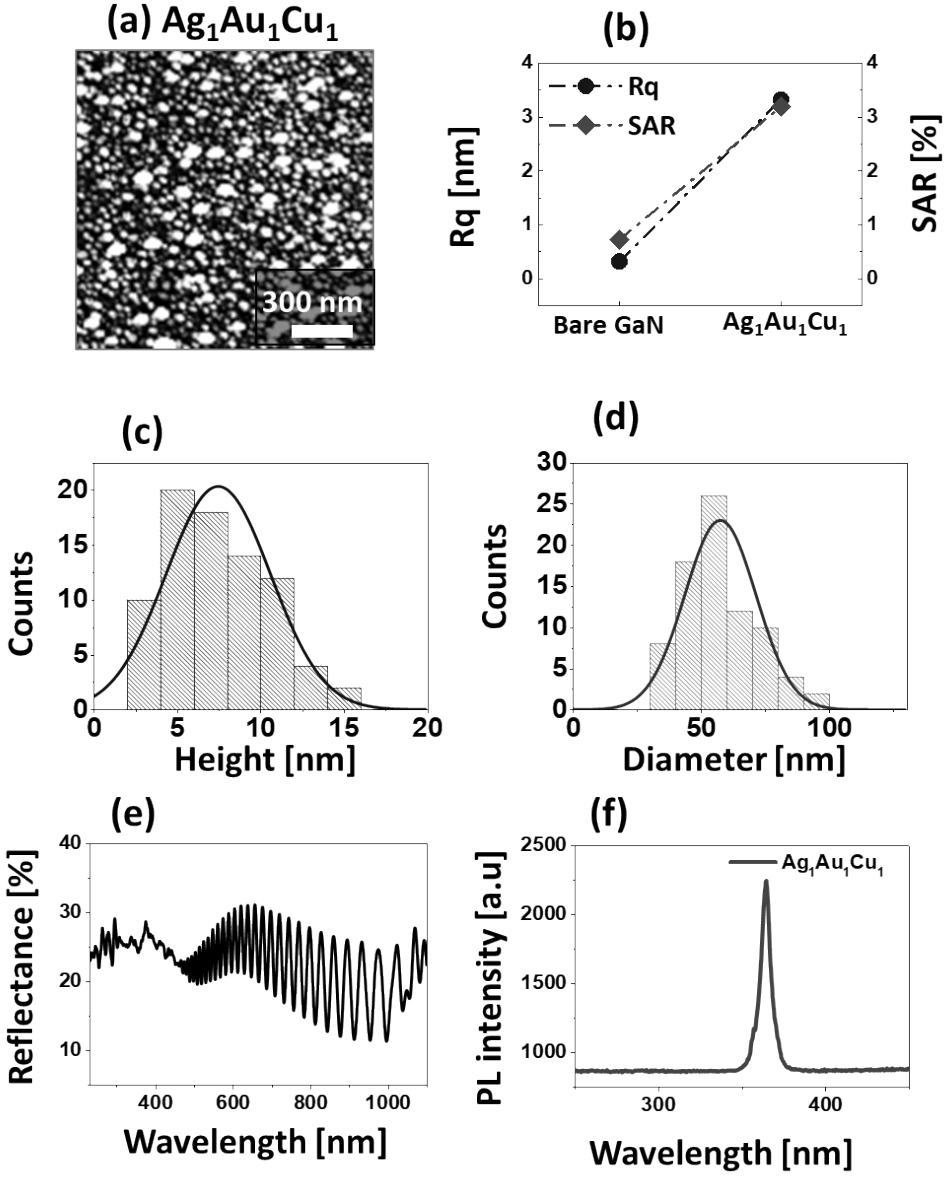

Figure S3: (a) AFM image of small AgAuCu alloy NPs on GaN fabricated at 500 ^{o}C for 120 s with the reduced thickness of tri-layer of $Ag_{1\ nm}/Au_{1\ nm}/Cu_{1\ nm}$. The sample is named as $Ag_1Au_1Cu_1$. (b) SAR and Rq comparison of small alloy NPs with the bare GaN. (c) – (d) Height and diameter histogram distributions of $Ag_1Au_1Cu_1$ alloy NPs. (e) – (f) Reflectance and PL spectra of small trimetallic alloy NPs.

EDS spectra of alloy NP on GaN

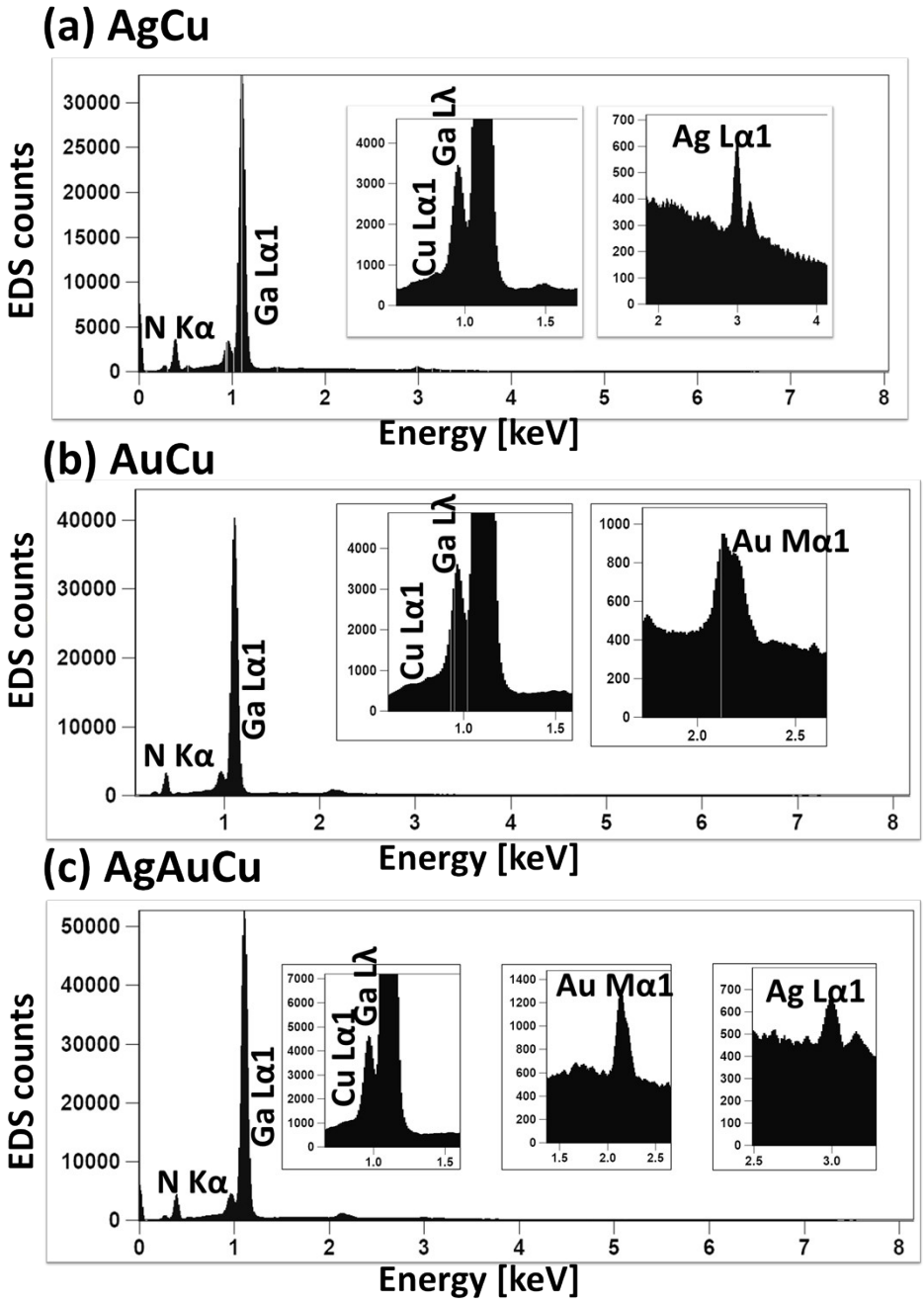

Figure S4: Elemental analysis of alloy NPs on GaN. (a) – (c) Energy dispersive x-ray spectroscope (EDS) spectra of alloy NPs fabricated with $Ag_{4\ nm}/Cu_{4\ nm}$, $Au_{2\ nm}/Cu_{2\ nm}$, and $Au_{2\ nm}/Au_{2\ nm}/Cu_{2\ nm}$ multilayers. Insets show the enlarged peak of each metal elements.

EDS spectra of multilayers on Si

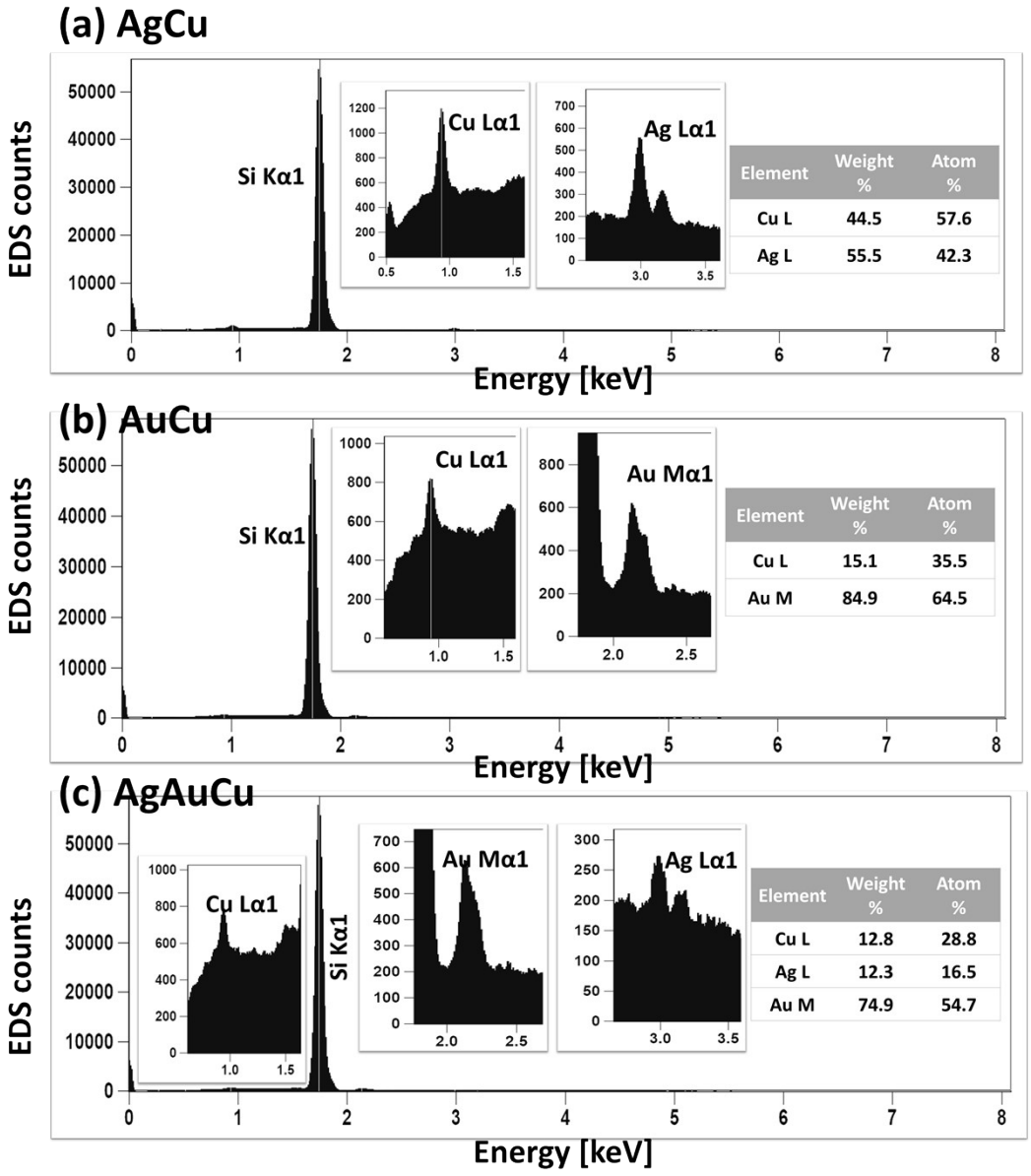

Figure S5: (a) – (c) EDS spectra of $Ag_{4\ nm}/Cu_{4\ nm}$, $Au_{2\ nm}/Cu_{2\ nm}$, and $Au_{2\ nm}/Au_{2\ nm}/Cu_{2\ nm}$ multilayers on Si substrates. Insets show the enlarged peaks and composition of Ag, Au and Cu. Since the Ga Lλ and Cu Lα1 peaks overlaps in the case of GaN substrate, the atomic % of alloy NPs was extracted using the same thickness of metallic layers on Si substrate.

Photoresponse of bare GaN PD

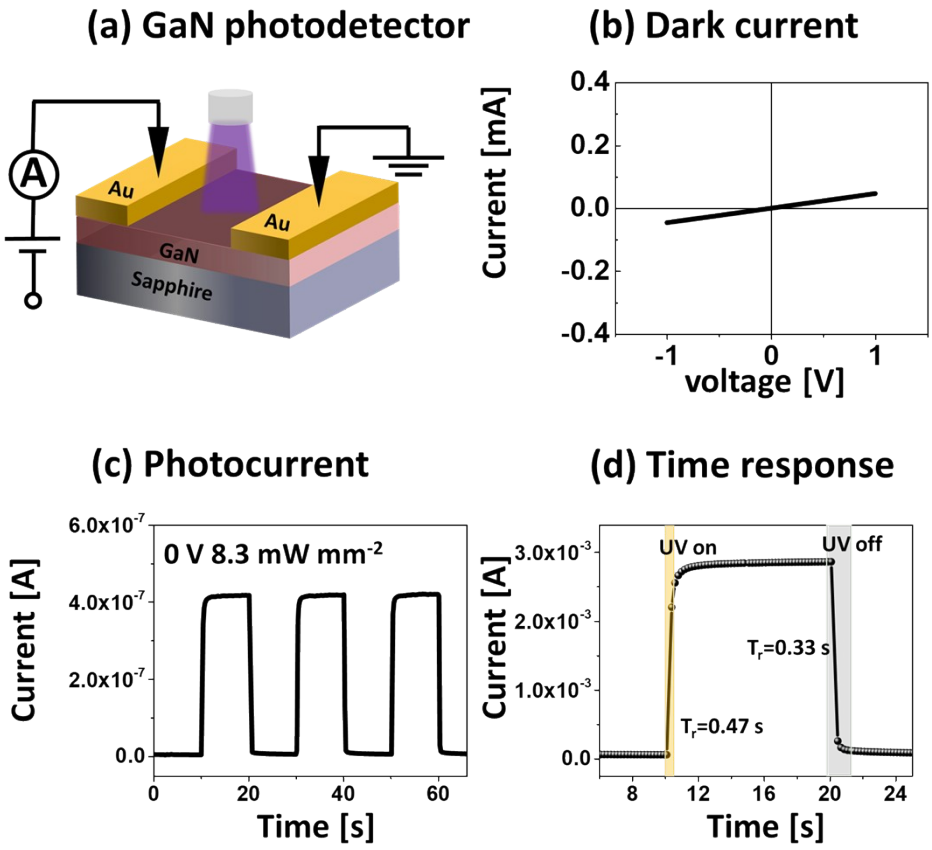

Figure S6: Photoresponse characteristic of bare GaN photodetector (PD) illuminated with 385 nm LED. (a) Schematic of bare GaN PD. (b) Dark current of bare GaN PD at 1 V. (c) Photocurrent at 0 V under 385 nm at 8.3 mW/mm^2. (d) Time response of bare GaN PD under 8.3 mW/mm^2 at 1 V.

Figure S6 shows the photoresponse characteristics of bare GaN photodetector (PD) under UV (385 nm) illumination at 1 V. The 100 nm-thick Au electrodes were deposited on GaN with the 200-µm wide active region as shown in Fig. S6(a). The dark current (I_{dark}) of bare GaN PD was 4.59 × 10^{-5} A in Fig. S6(b), demonstrating an ohmic contact behavior between the GaN and Au electrodes perhaps with the surface pinning effect with the linear characteristic [3]. At 0 V, the GaN demonstrated a photocurrent (I_{ph}) of 4.16 × 10^{-7} A upon the UV illumination of 8.3

mW/mm^2. The driven force of this self-power mode is due to the built-in e-field at the junction interface [4]. The potential for the typical metal-semiconductor junction is given by the Schottky Mott model: $\phi_s = \phi_m - \chi$; where the ϕ_s is semiconductor work function, the ϕ_m is the metal work function and the χ is electron affinity [3,5]. When Au electrode was deposited onto the epitaxial GaN layer, the potential barrier of depletion region can allow the inner electron-hole pairs to flow towards the electrodes at zero bias [5]. Therefore, the small I_{ph} can be observed by *I-V* measurement. The bare GaN PD demonstrated the rise (T_r) and fall (T_f) time of 0.47 s and 0.33 s under 8.3 mW/mm^2 at 1 V as seen in Fig. S6(d), suggesting a high quality GaN template [6].

Table S1: Summary of average diameter (AD), average height (AH), $R_{q,}$ and SAR of various alloy NPs and bare GaN. (Related to Fig. 3(d))

Samples	AD [nm]	AH [nm]	R_q [nm]	SAR [%]
Bare GaN	--	--	6.644	11.0733
AgCu	108.3	18.6	6.642	6.7236
AuCu	119.1	20.6	10.344	11.7028
AgAuCu	135.6	26.0	12.096	12.6827

Table S2: Summary of responsivity (*R*) of bare GaN and various alloy NP-based photodetectors as a function of power variation at 10 V. (Related to Fig. 5(g))

Power [mW/mm^2]	**Responsivity [A W^{-1}]**			
	Bare GaN	**AgCu NPs**	**AuCu NPs**	**AgAuCu NPs**
0.08	264.37	903.13	1652.5	4301.25
0.15	186.67	639.00	1191.00	2622.00
1.60	46.43	146.03	209.40	335.06
2.91	36.89	106.36	135.87	198.38
8.3	22.71	55.72	59.83	78.45
17.6	14.59	32.78	32.21	38.48
28.9	10.60	22.15	21.05	23.95
54.9	6.38	13.16	11.52	13.17

Table S3: Summary of external quantum efficiency (*EQE*) of bare GaN and various alloy NP-based photodetectors as a function of power variation at 10 V. (Related to Fig. 5(h))

Power [mW/mm²]	**EQE [%]**			
	Bare GaN	**AgCu NPs**	**AuCu NPs**	**AgAuCu NPs**
0.08	8.51×10^{4}	2.91×10^{5}	5.32×10^{5}	1.39×10^{6}
0.15	6.01×10^{4}	2.06×10^{5}	3.84×10^{5}	8.44×10^{5}
1.60	1.50×10^{4}	4.70×10^{4}	6.74×10^{4}	1.08×10^{5}
2.91	1.19×10^{4}	3.43×10^{4}	4.38×10^{4}	6.39×10^{4}
8.3	7.31×10^{3}	1.79×10^{4}	1.93×10^{4}	2.53×10^{4}
17.6	4.70×10^{3}	1.06×10^{4}	1.04×10^{4}	1.24×10^{4}
28.9	3.42×10^{3}	7.13×10^{3}	6.78×10^{3}	7.71×10^{3}
54.9	2.06×10^{3}	4.24×10^{3}	3.71×10^{3}	4.24×10^{3}

Table S4: Summary of detectivity (*D*) of bare GaN and various alloy NPs PD as a function of power variation at 10 V. (Related to Fig. 5(i))

Power [mW/mm^2]	Detectivity [jones]			
	Bare GaN	**AgCu NPs**	**AuCu NPs**	**AgAuCu NPs**
0.08	3.62×10^{11}	5.46×10^{11}	8.01×10^{11}	3.52×10^{12}
0.15	2.55×10^{11}	3.86×10^{11}	5.77×10^{11}	2.15×10^{11}
1.6	6.35×10^{10}	8.83×10^{10}	1.01×10^{11}	2.74×10^{11}
2.91	5.05×10^{10}	6.43×10^{10}	6.59×10^{10}	1.62×10^{11}
8.3	3.11×10^{10}	3.37×10^{10}	2.90×10^{10}	6.42×10^{10}
17.6	2.00×10^{10}	1.98×10^{10}	1.56×10^{10}	3.15×10^{10}
28.9	1.45×10^{10}	1.34×10^{10}	1.02×10^{10}	1.96×10^{10}
54.9	8.73×10^{9}	7.96×10^{9}	5.58×10^{9}	1.08×10^{10}

Table S5: Summary of *R*, *EQE,* and *D* of bare GaN and a different component of alloy NPs PD as a function of different wavelengths at 10 V. The light intensity is fixed at 1.60 mW/mm^2. (Related to Figs. 5(d) – 5(f))

Wavelength [nm]		Sample			
		Bare GaN	**AgCu NPs**	**AuCu NPs**	**AgAuCu NPs**
Responsivity [A W^{-1}]	**275**	43.31	180.47	208.59	338.31
	385	46.44	146.03	209.41	335.06
	455	0.99	18.22	1.61	52.92
	530	1.95	13.54	0.85	22.58
EQE [%]	**275**	1.95×10^{4}	8.14×10^{4}	9.41×10^{4}	1.5310^{5}
	385	1.50×10^{4}	4.70×10^{4}	6.74×10^{4}	1.08×10^{5}
	455	2.69×10^{2}	4.97×10^{3}	4.38×10^{2}	1.44×10^{4}
	530	4.56×10^{2}	3.17×10^{3}	1.98×10^{2}	5.28×10^{3}
Detectivity [jones]	**275**	5.92×10^{10}	1.09×10^{11}	1.01×10^{11}	2.77×10^{11}
	385	6.35×10^{10}	8.83×10^{10}	1.00×10^{11}	2.74×10^{11}
	455	1.35×10^{9}	1.10×10^{10}	7.79×10^{8}	4.33×10^{10}
	530	2.66×10^{9}	8.19×10^{9}	4.10×10^{8}	1.85×10^{10}

References:

1 P. B. Johnson and R. W. Christy, *Phys. Rev. B*, 1972, **6**, 4370–4379.

2 A. R. Beal and H. P. Hughes, *J. Phys. C Solid State Phys.*, 1979, **12**, 881–890.

3 Y. Liu, J. Guo, E. Zhu, L. Liao, S.-J. Lee, M. Ding, I. Shakir, V. Gambin, Y. Huang and X. Duan, *Nature*, 2018, **557**, 696–700.

4 K. M. Tracy, P. J. Hartlieb, S. Einfeldt, R. F. Davis, E. H. Hurt and R. J. Nemanich, *J. Appl. Phys.*, 2003, **94**, 3939–3948.

5 S. K. Jain, N. Aggarwal, S. Krishna, R. Kumar, S. Husale, V. Gupta and G. Gupta, *J. Mater. Sci. Mater. Electron.*, 2018, **29**, 8958–8963.

6 R. Zhuo, Y. Wang, D. Wu, Z. Lou, Z. Shi, T. Xu, J. Xu, Y. Tian and X. Li, *J. Mater. Chem. C*, 2018, **6**, 299–303.